RSC Advances

ROYAL SOCIETY OF CHEMISTRY

www.rsc.org/advances

Cite this: DOI: 10.1039/c0xx00000x

www.rsc.org/xxxxxx

ARTICLE TYPE

Sandwich-structured MnO_2/polypyrrole/reduced graphene oxide hybrid composites for high-performance supercapacitors

Guangqiang Han,[a] Yun Liu,[a] Erjun Kan,[b] Jian Tang,[a] Lingling Zhang,[a] Huanhuan Wang,[a] Weihua Tang*[a]

Received (in XXX, XXX) Xth XXXXXXXXX 20XX, Accepted Xth XXXXXXXXX 20XX
DOI: 10.1039/b000000x

The rational preparation of hierarchical MnO_2/polypyrrole (PPy)/reduced graphene oxide (rGO) nanosheets in a sandwich structure is presented. By co-assembly of MnO_2/GO and PPy/GO into layer-by-layer architecture and reduction of GO, ternary (MnO_2, PPy)/rGO composites were first fabricated. The materials were fully characterized in terms of structure, morphology and electrochemical properties. The unique architecture offers the composites good capacitance by taking advantage of the strong synergistic effect of each component. A maximum specific capacitance as high as 404 F g^{-1} was obtained for this composite electrode. And over 91% of the initial capacitance was retained after continuous 5000 cycling. The good electrochemical performance and long-term cycling stability make this approach attractive in developing multifunctional hierarchical composites for high-performance supercapacitors.

1. Introduction

New types of energy storage devices have been attracting tremendous attention because of energy shortage and environmental concerns.[1] Among the various energy systems in study, electrochemical capacitor (or supercapacitors) exhibit superior properties over batteries in terms of their high power density, fast charging/discharging rate, long cycle life and excellent reversibility.[2-4] The supercapacitors mainly compose of electrodes, electrolyte and separator. The cathode has a great impact on the supercapacitor performance. Many potential candidates for cathodes have been studied, which include carbonaceous materials, conducting polymers and transition metal oxides.[5-8] Graphene, one kind of carbonaceous material with high specific surface area and excellent conductive properties,[9,10] exhibits a large and stable double layer capacitance. The easy agglomeration and stacking of graphene sheets however, limit their application in high energy density supercapacitors.[11] Conducting polymers and transition metal oxides are typical pseudocapacitive materials. Their poor stability and high resistance during cycling, however, limit their practical applications as electrodes. The hybrid composites of graphene with conducting polymers and/or transition metal oxides have demonstrated as promising candidates for high-performance supercapacitors.[12-14]

As the most promising transition metal oxide[15] for the next generation of supercapacitors, manganese oxide (MnO_2) has received considerable attention due to its high-energy density, low cost, environmental friendliness, natural abundance, and high theoretical specific capacitance as high as 1370 F g^{-1}.[16] However, bulk MnO_2 usually deliver low specific capacitance (50-250 F g^{-1}) and poor charging/discharge rate,[16] due to poor electrical conductivity and electrochemical dissolution during cycling.[17] To solve this problem, carbonaceous materials (including graphene, carbon nanotube and carbon fibers) and conductive polymers have been employed as matrices for MnO_2-based electrode materials to improve their electrical conductivity and stability.[18-24] Gaphene is emerging as one of the most appealing carbon matrices, due to its unique properties in electrical conductivity, mechanical flexibility and chemical stability.[25] In the preparation of hybrid materials for supercapacitor cathodes, nanostructured MnO_2/graphene based composites have been explored. By co-assembly of honeycomb MnO_2 nanospheres between graphene nanosheets, a graphene-wrapped MnO_2 nanocomposites was prepared to deliver a specific capacitance of 210 F/g at 0.5 A/g current density.[24] By reducing functionalized graphene oxide with poly(diallyldimethylammonium chloride), Zhang et al. prepared a layer-structured composite by co-deposition of reduced graphene oxide (rGO) with MnO_2 nanosheets, where enhanced capacitive performances was observed with this MnO_2/rGO nanosheet composite than those of pure functionalized rGO.[26] Cheng et al.[27] further an asymmetric electrochemical capacitor, where graphene was used as cathode and a MnO_2 nanowire/graphene composite as the anode. The retention of specific capacitance for the supercapacitor was 89%[26] and ~79%,[27] respectively.

The binary composites of graphene with conductive polymers such as polypyrrole and polyaniline have also shown unique electronic and electrochemical properties.[28,29] For graphene-polymer composites, it was reported that improved electronic and thermal conductivities were obtained when GO was reduced into rGO.[30] Recently, MnO_2/graphene based ternary composites have been further developed by wrapping the nanostructure with carbon nanotube or conductive polymers [ca. polyaniline and poly(3,4-ethylenedioxythiophene):poly(styrenesulfonate)].[31] The ternary composite electrode delivered a highest specific capacitance of high as ~380 F/g, which was 20% or 45% higher than the binary composite electrode.

In continuation of our recent pursue of robust high-performance supercapacitors,[9,32-34] we are inspired to propose new approaches to develop structure-defined ternary composites of graphene, MnO_2 and conductive polymers. In this work, a co-assembly approach to prepare (MnO_2, PPy)/rGO ternary hybrid nanocomposite (GMP) is proposed. By taking advantage of the functionality and aqueous dispersability of GO, aqueous MnO_2/GO and polypyrrole/GO dispersions were prepared individually and allowed to co-assembly into ternary composites with the aid of ultrasonication. As described in Fig. 1, the layer-by-layer sandwich-structured GMP composite was successfully achieved. The hybrid nanostructured composite based cathode delivered a maximum specific capacitance of 404 F g^{-1} at 0.25 mA g^{-1}, with a capacitance retention over 91% obtained over 5000 cycling in supercapacitor.

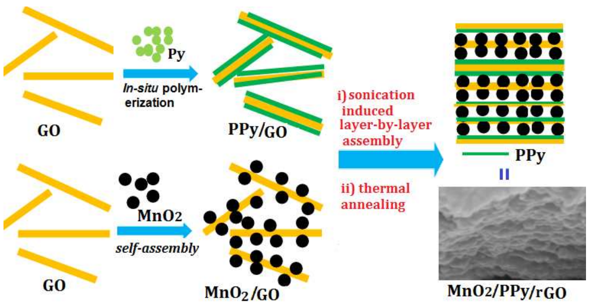

Fig. 1 Schematic illustration for formation of (MnO_2, PPy)/rGO composites.

2. Experimental section

2.1. Preparation of MnO_2/PPy/rGO (GMP) nanocomposites

All chemicals and reagents were obtained from commercial sources and were analytical grade. Pyrrole (Py) was distilled prior to use. GO and MnO_2 nanostructures were prepared with the methods in literature.[9,35]

The MnO_2/PPy/rGO sandwich-structure nanocomposites were prepared using sonication-induced assembly of aqueous dispersions of both MnO_2/rGO and PPy/rGO composite. Both MnO_2/rGO and PPy/rGO composites were synthesized separately with the following procedures. GO (0.06 g) dispersion in de-ionized (DI) water (100 mL), was ultrasonicated for 1 h to obtain a yellow-brown suspension. The suspension was then added with a MnO_2 (0.6 g) dispersion in water.[35] The resulting mixture was further ultrasonically dispersed for 30 min to obtain a dark brown dispersion. The dispersion was filtered, rinsed with DI water and alcohol to afford MnO_2/GO composite. The composite was dispersed in DI water (100 mL) for use.

The PPy/GO composite was prepared according to our reported procedure.[9] The yellow-brown suspension of GO (0.06 g) in distilled water (100 mL) was ultrasonicated for 1 h. The suspension was then added with pyrrole (Py, 0.2 g) and sonicated at 0 ~ 5 °C for another 30 min. $FeCl_3$ solution (0.49 g in 1 M HCl) was then slowly added. The reaction was maintained at 0 ~ 5 °C for 24 h. After filtration, the PPy/GO composite was collected and washed with ethanol and DI water twice. The PPy/GO dispersion in DI water (100 mL) was prepared for use.

The as-obtained MnO_2/GO and PPy/GO dispersions in DI water (100 mL) were mixed and ultrasonicated for 1 h. The resulting hybrid composite was filtered and washed with ethanol and distilled water before drying at 60°C for 24 h. The samples were then heated at 150°C in vacco for 1 h to reduce GO into rGO to afford the *titled* GMP composites. For comparison, the MnO_2/GO nanocomposite was also heated at 150°C in vacco to prepare MnO_2/rGO composites.

2.2. Material characterization

Samples were characterized in terms of structure and morphology. Fourier transform infrared spectroscopy (FT-IR) analyses were carried out on a Bomen MB154S Fourier transform infrared. Raman spectra were collected on a Renishaw laser confocal Raman spectrometer employing a 532 nm laser beam. X-ray diffraction (XRD) patterns were recorded on an X-ray diffractometer (D8 Advance, Bruker, Germany) by using Cu Kα radiation (λ=1.54 Å) at 40 kV and 30 mA. X-ray photoelectron spectroscopy (XPS) analyses were performed on a Thermo ESCALAB 250 instrument. Transmission electron microscopy (TEM) images were observed on a JEOL JEM-2100 microscope. Field emission gun scanning electron microscopy (FE-SEM) images were observed on a Hitachi S4800 FESEM at an accelerating voltage of 15 kV.

2.3. Electrochemical measurement

The electrochemical properties of all as-prepared composites were evaluated with a CHI660D electrochemical workstation (Shanghai, China) in 1M Na_2SO_4 solutions at room temperature. The working electrodes were prepared by the following method: the polytetrafluoroethylene, 15 wt% acetylene black and ethylene solution were added to the composites to produce a homogeneous paste and then pressed onto nickel foam current collectors, after that, the electrodes was dried under vacuum at 60°C for 24 h. The electrochemical performance of composites was studied with cyclic voltammetry (CV), galvanostatic charge–discharge and electrochemical impedance spectroscopy (EIS) techniques. CV measurements were performed in voltage range of -0.3 ~ 0.5 V at scan rate of 10, 20, 30, 40, 50 and 100 mV/s, respectively. Charge-discharge measurements were carried out galvanostatically at 0.25~4 A/g scan rate over voltages ranging from -0.3 V to 0.5 V. EIS was operated in a frequency range of $1 \times 10^5 \sim 1 \times 10^{-2}$ Hz at 0.5 V with an AC voltage amplitude of 50 mV.

3. Results and discussion

3.1. Structure characterization

The structure of the as-prepared GMP composite was confirmed with FT-IR, Raman, XRD and XPS spectroscopy. Fig. 2a shows the FT-IR spectra of GO, rGO, MnO_2, MnO_2/rGO, PPy and (MnO_2, PPy)/rGO. The FT-IR spectrum of GO shows the presence of various oxygen-containing groups, i.e., the peak at 3438 cm^{-1} corresponding to –OH, while the peaks at 1730 cm^{-1} and 1060 cm^{-1} assigned to carboxy (COOH) and epoxide (C–O–C) respectively. The peak at 1625 cm^{-1} can be attributed to the C=C stretching vibration.[36] Compared with GO, the peak corresponding to –OH (at 3438 cm^{-1}) disappeared in the FT-IR spectrum of RGO, while the peaks at 1730 cm^{-1} and 1060 cm^{-1} weakened, indicating most GO was successfully reduced into rGO after 150°C heating in vacco for 1 h.[37] For PPy, the characteristic absorptions were observed for peaks at 3428 cm^{-1} and 1542 cm^{-1}, attributed to the N-H and C=C stretching vibration in pyrrole ring, respectively. The peaks at 1298 cm^{-1} and 1162 cm^{-1} correspond to the C–H and C–N in-plane ring deformation and bending modes.[32] For the spectrum of GMP, all identical characteristic vibrations of MnO$_2$/rGO composite were clearly observed. Besides, the incorporation of PPy led to some peaks of PPy slightly shifted to high wavenumber, e.g., the peak at 1298 cm^{-1} in PPy shifted to 1320 cm^{-1} in GMP. All results suggests that the successful intercalation of MnO$_2$ and PPy into rGO nanosheets during the modification process.

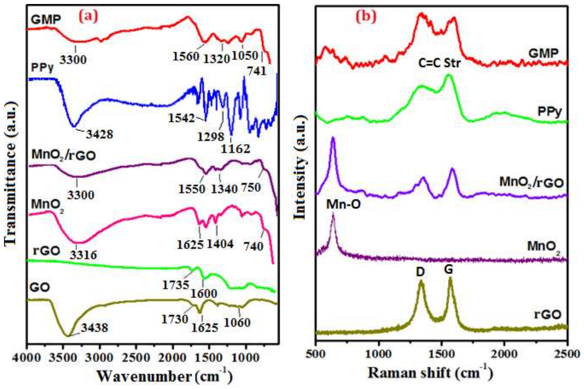

Fig. 2 (a) FT-IR spectra (b) Raman spectra of rGO, MnO$_2$, MnO$_2$/rGO, PPy and GMP.

Fig. 2(b) shows the Raman spectra of rGO, MnO$_2$, MnO$_2$/rGO, PPy and GMP. The rGO exhibits two characteristic peaks, i.e., one at 1335 cm^{-1} for D band and another at 1576 cm^{-1} for G bands. The D band is associated with the first-order Raman scattering of the E_{2g} vibrational mode and the G band corresponds to sp^2-bonded carbon atoms.[38] MnO$_2$ presents a characteristic peak at 634 cm^{-1} for the Mn-O lattice vibrations. The MnO$_2$/rGO composite presents all above-mentioned characteristic peaks of rGO and MnO$_2$. PPy shows a characteristic peak at 1555 cm^{-1}, corresponding to its C=C stretching vibration.[39] As clearly shown in the Raman spectra of GMP, all characteristic peaks for RGO, MnO$_2$ and PPy are observed. Only the peak for MnO$_2$ weakened in intensity.

Fig. 3(a) shows XRD patterns of rGO, MnO$_2$, MnO$_2$/rGO, PPy and GMP. The rGO exhibits a broad peak centered at 25°, corresponding to an interlayer spacing of 0.776 nm.[34] This peak is formed due to deep reduction of GO, indicating most oxygen functional groups had been removed.[20,37] For MnO$_2$ nanospheres, significant XRD peaks were observed at $2\theta = 12.4$, 25.3, 37.2 and 65.8°, which can be well-assigned to the (001), (002), (100) and (110) planes of birnessite-type MnO$_2$, respectively.[18,35] From $2\theta = 12.4°$, the interlayer spacing for MnO$_2$ was calculated to be 0.72 nm, in good agreement with the literature.[40] The MnO$_2$/rGO nanocomposites show a similar XRD pattern as MnO$_2$. The sample of pure PPy exhibits a broad diffraction peak at $2\theta = 25.2°$, which was the characteristic peak of amorphous PPy.[32] For the pattern of GMP, no obvious peak of graphite at 26.6° can be found, suggesting that the agglomeration of graphene sheets was successfully inhibited by MnO$_2$ and PPy nanostructures depositing on their surfaces. All characteristic peaks of rGO, MnO$_2$ and PPy were observed, indicating the co-assembly process with low addition of rGO (ca. 10 wt%) does not affect the crystal structure of MnO$_2$ nanospheres.

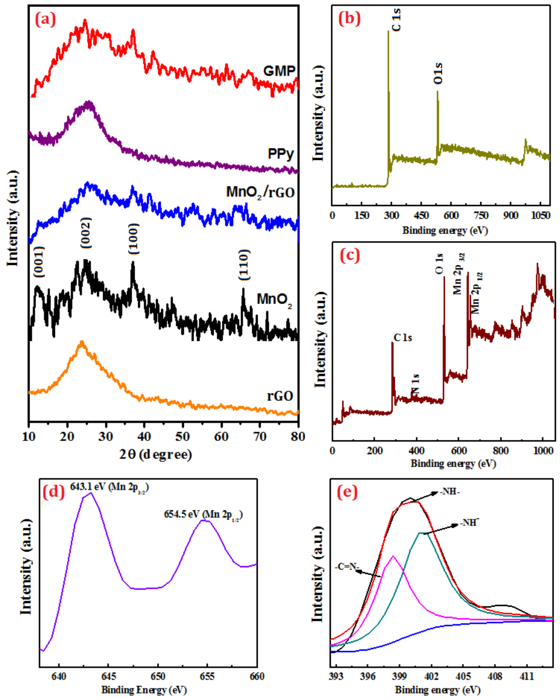

Fig. 3 (a) XRD patterns of rGO, MnO$_2$, MnO$_2$/rGO, PPy and GMP. XPS spectra of (b) rGO, (c) GMP, (d) Mn 2p for GMP and (e) N 1s for GMP.

A surface elemental analysis was further conducted on he rGO and GMP nanocomposites using X-ray photoelectron spectroscopy (XPS). The XPS spectrum of rGO (Fig. 3(b)) exhibits the signal for O element, indicating the remaining of oxygen functional groups even after deep reduction of GO. The full spectrum of GMP shows the signals from C, N, O and Mn, suggesting the presence of MnO$_2$ and PPy on rGO surfaces. The high-resolution Mn 2p core level spectrum (Fig. 3(d)) shows the binding energies centered at 643.1 and 654.5 eV for Mn 2p$_{3/2}$ and Mn 2p$_{1/2}$, respectively, together with a spin-orbit splitting of 11.4 eV.[41] The results are in good agreement with the reported data for MnO$_2$.[42] The high-resolution N 1s of core level spectrum (Fig. 3(e)) could be deconvoluted into three Gaussian peaks with the binding energy of 398.3, 400.2 and 401.1 eV, corresponding to the imine-like structure (–C=N–), the neutral and amine-like structure (–NH–) and positively charged structure (–NH$^+$–). The deconvoluted results are in good accordance with the data in literarure.[32,43] The XPS analysis further confirmed the existence of rGO, MnO$_2$ and PPy in GMP nanocomposites.

3.2. Morphology observation

The morphology of rGO, MnO$_2$, MnO$_2$/rGO$_2$, PPy and GMP nanocomposites were observed using TEM and FE-SEM observations. The TEM image of rGO (Fig. 4(a)) shows the thin layer structure with smooth surfaces.[44] The pristine MnO$_2$ samples shows severe aggregation of MnO$_2$ nanospheres (Fig.

4(b)). The aggregation of MnO_2 nanospheres can be significantly inhibited in MnO_2/rGO composites (Fig. 4(c)). The MnO_2 phases well dispersed on the surface of rGO nanosheets. Fig. 4(d) shows the TEM image of aggregated state of pristine PPy. After co-assembly of MnO_2/rGO and PPy/rGO dispersion in water, the (MnO_2, PPy)/rGO ternary hybrid composites exhibited a layer-by-layer structure, where MnO_2/rGO and PPy/rGO layers sandwiched to form compact intercalated graphene composites (Fig. 4(e)). The PPy, MnO_2 and RGO can be clearly observed in the TEM image of GMP composites, where PPy and MnO_2 phases were deposited on exfoliated rGO nanosheets. The formation process of GMP layered structure is illustrated as in Fig. 4(f), where two kinds of surface-deposited rGO nanosheets assembled to form the sandwich-structure composites. The surface morphology of GMP is shown as Fig. 4(g), where MnO_2 particles or PPy particles deposited on the surface of rGO sheets. The layered structure can be confirmed with the section-view morphology of the ternary composites. Crinkled rGO nanosheets were well exfoliated by surfaced-deposited MnO_2 and PPy particles. The flexible and ultrathin (ca. 10 nm) rGO sheets wrapped the MnO_2 and PPy particles, which would help to not only enhance the electrical conductivity of the ternary composites but also prevent MnO_2 phases from aggregation and electrical dissolution.[18]

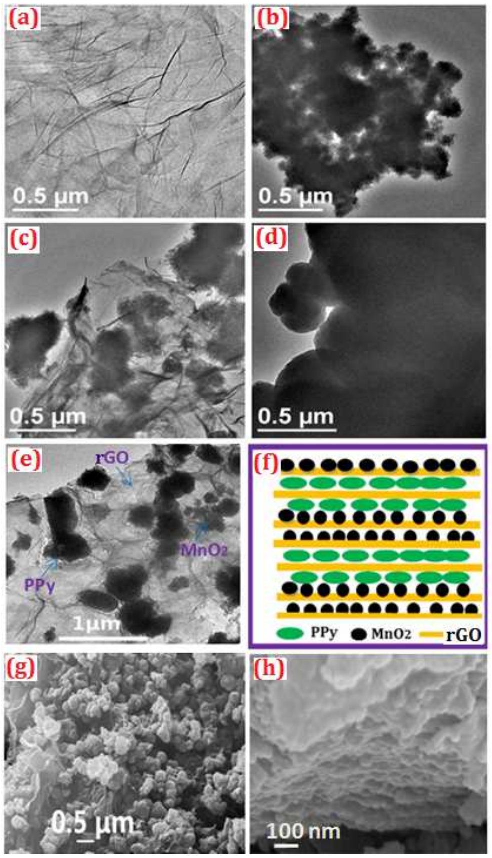

Fig. 4 TEM images of (a) rGO, (b) MnO_2, (c) MnO_2/rGO, (d) PPy and (e) GMP. (f) Schematic illustration of GMP. FE-SEM images of (g) GMP and (h) GMP at cross-section.

On the basis of the above analyses, it is reasonable to conclude that layer-by-layer (MnO_2, PPy)/rGO composites were successfully prepared. The coassembly process may be driven by the electrostatic interactions and hydrogen bonding.[18,32] From TGA analysis, the weight fraction of MnO_2, PPy and rGO in the ternary composites was determined to be 44.8%, 45.6% and 9.6%, which is very similar to the feeding fraction of MnO_2 (45%), PPy (45%) and rGO (10%) in the preparation of the hybrid composites. Such high contents of MnO_2 and PPy particles wrapped by flexible crinkled rGO nanosheets as conductive pathway and protecting matrix might result in high capacity and good cycling performance when used as cathode in supercapacitors.

3.3. Electrochemical properties

The capacitive performance of electrode materials was evaluated using cyclic voltammetry (CV) and galvanostatic charge-discharge techniques in 1 M Na_2SO_4 aqueous solutions. Fig. 5(a) shows the CV curves of GMP at different scan rates. The nearly rectangle-shaped and symmetric CV curves at low scan rates indicate the fast reversible Faradic reactions and perfect capacitive behavior of GMP electrodes. With the increase of scan rate, the CV curves gradually deviated from rectangular shape. This behavior may be explained with the charge-discharge process of composites in Na_2SO_4 aqueous electrolyte, which is associated with the insertion of Na^+ into hybrid material and release of Na^+ from the composite to the electrolyte.[18] At a low scan rate (ca. 10 mV s^{-1}), the Na^+ ions can easily diffuse into all accessible spaces of the hybrid composite. At a high scan rate of 100 mV s^{-1}, the Na^+ ions can only reach the outer surface of the hybrid material and the internal part of the material has little contribution to the electrochemical capacitive behavior.

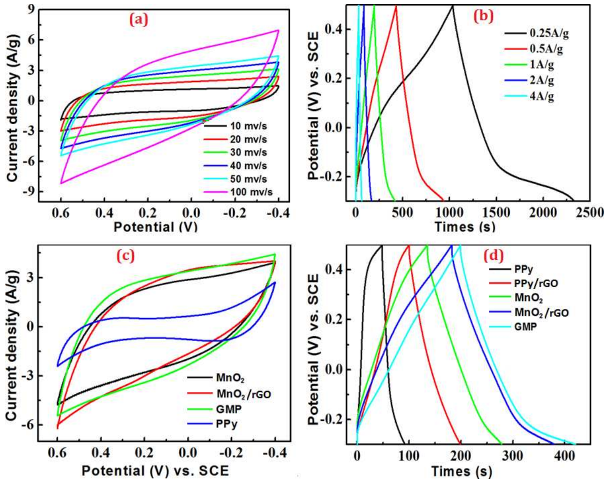

Fig. 5 (a) CV curves of (a) GMP at different scan rates, (b) charge-discharge curves of GMP at different current densities, (c) CV curves of MnO_2, MnO_2/rGO, GMP and PPy at 50 mV/s scan rate, and (d) Charge-discharge curves of PPy, PPy/rGO, MnO_2, MnO_2/rGO and GMP at 1 A/g.

Fig. 5(c) presents the CV curves of MnO_2, MnO_2/rGO, GMP and PPy electrodes at scan rate of 50 mV s^{-1}. GMP exhibits the largest area for the closed CV loop than the rest electrodes, indicating the highest capacitance achieved from GMP composites. Fig. 5(b) shows the galvanostatic charge-discharge curves of GMP at different current densities. The discharge time decreased with the increase of current density. During the charge and discharge process, the charge curve of GMP is almost symmetric to its corresponding discharge counterpart with a slight curvature, suggesting the high reversibility of the hybrid materials. The specific capacitances (Cs) can be calculated according to the equation Cs = (It)/(mV),[45] where I is the charge-discharge current (A), V the potential window (V), t the discharge time (s) and m the mass of the active material (g). The specific capacitance of GMP was calculated to be 404 F g^{-1} at current density of 0.25 A g^{-1}. The value could maintain as high as 120 F g^{-1} even at 4 A g^{-1}, suggesting the potential of GMP as electrode materials. A close look at the galvanostatic charge-discharge curves of PPy, PPy/rGO, MnO_2, MnO_2/rGO and GMP in Fig. 5(d), one would calculate the specific capacitance of GMP as 283.4 F g^{-1}, in contrast to 243.6 F g^{-1} for MnO_2/rGO_2 and 54.5 F g^{-1} for PPy. The superior performance of GMP can be attributed to the strong synergistic effect between the components. The co-assembly process brought the mutual combination of conducting MnO_2 and PPy onto rGO sheets at nanoscale level. The compact structure offered the close interactions between MnO_2 and PPy, where electron shuttling along PPy mainchains and inter-chain hopping in pristine PPy can be avoided.[19] The effective electron transport to rGO sheets was thus facilitated with the built-in continuous conductive network for fast charge collection and transfer across the electrode. On the other hand, the MnO_2 and PPy particles with an intimate electrical connection to GO sheets offered short ion diffusion and electron transfer pathways, enabling maximum utilization of each component.

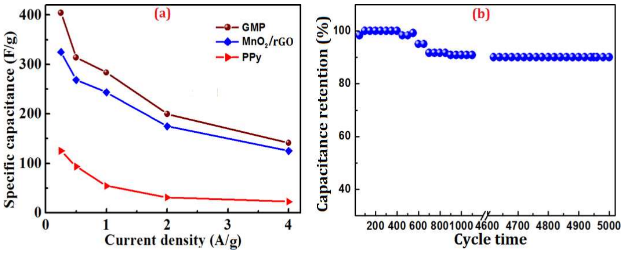

Fig. 6 (a) Specific capacitance of MnO_2/rGO, PPy, GMP at different current densities, and (b) the capacitance retention of GMP over 5000 cycles at current density of 4A/ g.

Fig. 6(a) further compares the specific capacitance values of GMP with MnO_2/rGO and PPy at different current densities (0.25 - 4 A g^{-1}). It is evident that GMP possessed much higher capacitance than other composites at the same current density in the range, which is ascribed to the synergetic contribution of rGO, MnO_2 and PPy within the unique sandwich structure. The specific capacitances of all electrodes decreased with the increment of current density. The low specific capacitances at high current density may be explained with the insufficient contact of Na^+ ions with the composite in electrolyte. The electrochemical stability of the composite electrodes is crucial for long-term service in supercapacitors. The cycling performance of GMP electrode was evaluated in CV for continuous cycles in the range of -0.3−0.5 V at 4 A g^{-1}. As shown in Fig. 6(b), in the first 200 cycles, the specific capacitance maintained during the first 500 cycles. GMP exhibited decreased specific capacitance with cycling time before a plateau of capacitance was achieved. The capacitance retention of GMP was high as about 91% even after 5000 cycles, suggesting excellent cycling stability of GMP electrode. Such good cycling stability can be explained by the sandwich structure, i.e., high ion mobility channels were formed due to the improved conductivity with rGO and the uniformly dispersed MnO_2 and PPy on rGO sheets could prevent the stack of rGO.

The synergistic effect in the ternary (MnO_2, PPy)/rGO hybrid composite is further confirmed with electrochemical impedance spectroscopy (EIS). The ideal Nyquist impedance plot contain a half semicircle at high frequency and a straight line at low frequency, the high frequency part is related to solution resistance (R_s) and the width of the semicircle corresponds to the real impedance such as ionic charge-transfer resistance (R_{ct}) of composite layer on electrode.[46] Large diameter of the semicircle reveals high charge-transfer resistance and thus poor conductivity. Fig. 7 presents the Nyquist plots of MnO_2, MnO_2/rGO, PPy and GMP tested in 1 M Na_2SO_4. From the diameter of the semicircle, the charge-transfer resistance of MnO_2, MnO_2/rGO, PPy and GMP was calculated to be 13.5, 3.1, 2.2 and 1.5 Ω, respectively. The high resistance of pristine MnO_2 indicates its poor conductive property. The lowest resistance obtained for GMP may be explained with the synergic effect between rGO, MnO_2 and PPy, which affords efficient pathways for ion diffusion and electron transfer throughout the electrode.

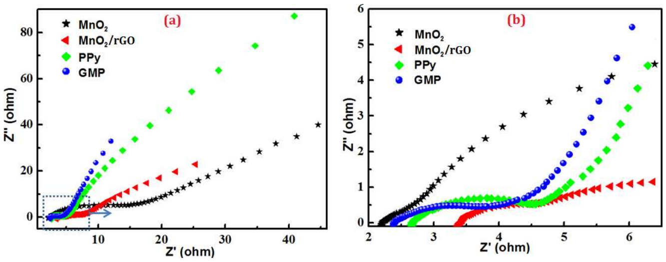

Fig. 7 (a) Nyquist plots of the EIS for GMP and (b) the magnified part of the semicircles.

4. Conclusions

In summary, (MnO_2, PPy/rGO) ternary composites are prepared in a sandwich structure with a co-assembly approach. By incorporating the multifunctional MnO_2 and PPy particles into rGO nanosheets, a unique hierarchical architecture is achieved. Such a structure enables the ternary composites to exhibit excellent electrochemical performance, much better than the individual components and their binary composites. The superior capacitance performance of ternary composites is attributed to the synergetic contribution of both conducting materials and the sandwich conductive network. The maximum specific capacitance of this ternary composite reaches 404 F/g at 0.25 A g^{-1}. Excellent capacitance retention was also observed for the ternary composites, where 91% of the original capacitance retained after 5000 cycles of charge−discharge process. The proposed approach demonstrates the incorporation of multifunctional components into conductive matrix to construct sandwich structure is efficient to realize high electrochemical performance with long cycling stability.

Acknowledgment

This research project was financially supported by the National Natural Science Foundation of China (Grant No. 21074055), Program for New Century Excellent Talents in University (Grant No. NCET-12-0633), Jiangsu Province Natural

Science Fund for Distinguished Young Scholars (Grant No. BK20130032), Doctoral Fund of Ministry of Education of China (Grant No. 20103219120008), and the Fundamental Research Funds for the Central Universities (Grant No. 30920130111006).

Notes and references

[a]*Key Laboratory of Soft Chemistry and Functional Materials, Ministry of Education, Nanjing University of Science and Technology, Nanjing 210094, P. R. China, Fax: +86 25 8431 7311; Tel: +86 25 8431 7311; E-mail: whtang@mail.njust.edu.cn*
[b]*Department of Applied Physics, Nanjing University of Science and Technology, Nanjing 210094, P. R. China*

1 X. Zhao, B. M. Anchez, P. J. Dobson and P. S. Grant, *Nanoscale*, 2011**, 3**, 839.
2 L. L. Zhang and X. S. Zhao, *Chem. Soc. Rev.,* 2009, **38**, 2520.
3 M. D. Stoller, S. Park, Y. Zhu, J. An and R. S. Ruoff, *Nano Lett.,* 2008, **8**, 3498.
4 M. Winter and R. J. Brodd, *Chem. Rev.*, 2004, **104**, 4245.
5 T. Brousse, M. Toupin, R. Dugas, L. Athouel, O. Crosnier and D. Blanger, *J. Electrochem. Soc.*, 2006, **153**, A2171.
6 H. Chen, S. Zhou, M. Chen and L. Wu, *J. Mater. Chem.*, 2012, **22**, 25207.
7 D. W. Wang, F. Li and H. M. Cheng, *J. Power Sources*, 2008, **185**, 1563.
8 N. L. Wu, *Mater. Chem. Phys.*, 2002, **75**, 6.
9 Y. Liu, H. Wang, J. Zhou, L. Bian, E. Zhu, J. Hai, J. Tang and W. Tang, *Electrochim. Acta*, 2013,**112**, 44.
10 D. Chen, H. Feng and J. Li, *Chem. Rev.*, 2012, **112**, 6027.
11 M. N. Patel, X. Wang, B. Wilson, D. A. Ferrer, S. Dai, K. J. Stevenson and K. P. Johnston, *J. Mater. Chem.*, 2010, **20**, 390.
12 Y. Hou, Y. Cheng, T. Hobson and J. Liu, *Nano Lett.*, 2010, **10**, 2727.
13 L. Mao, K. Zhang, H. S. O. Chan and J. Wu, *J. Mater. Chem.*, 2012, **22**, 1845.
14 Z. Li, J. Wang, X. Liu, S. Liu, J. Ou and S. Yang, *J. Mater. Chem.*, 2011, **21**, 3397.
15 R. Jiang, T. Huang, Y. Tang, J. Liu, L. Xue, J. Zhuang and A. Yu, *Electrochim. Acta*, 2009, **54**, 7173.
16 W.Wei, X. Cui, W. Chen, and D. G. Ivey, *Chem. Soc. Rev.*, 2011, **40**, 1697.
17 A. E. Fischer, K. A. Pettigrew, D. R. Rolison, R. M. Stroud and J. W. Long, *Nano Lett.*, 2007, **7**, 281.
18 J. Zhu and J. He, *ACS Appl. Mater. Interfaces*, 2012, **4**, 1770.
19 J. Wang, Y.Yang, Z. Huang and F. Kang, *J. Mater. Chem.,* **2012**, *22*, 16943.
20 J. Yan, Z. Fan, T. Wei, W. Qian, M. Zhang, F. Wei, *Carbon*, 2010, **48**, 3825.
21 G. Yu, L. Hu, N. Liu, H. Wang, M. Vosgueritchian, Y. Yang, Y. Cui and Z. Bao, *Nano Lett*., **2011**, *11*, 4438.
22 G. Yu, L. Hu, M. Voshueritchian, H. Wang, X. Xie, J. M. McDonough, X. Cui, Y. Cui and Z. Bao, *Nano Lett.,* **2011**, *11*, 2905.
23 G. Wang, Q. Tang, H. Bao, X. Li and G.Wang, *J. Power Sources,* **2013**, *241*, 231.
24 Y. Hou, Y. Cheng, T. Hobson and J. Liu, *Nano Lett*., **2010**, *10*, 2727.
25 K. S. Novoselov, A. K. Geim, S. V. Morozov, D. Jiang, Y. Zhang, S. V. Dubonos, I. V. Grigorieva and A. A. Firsov, *Science,* 2004, **306**, 666.
26 J. Zhang, J. Jiang, and X. S. Zhao, *J. Phys. Chem. C*, 2011, **115**, 6448.
27 Z. Wu, W. Ren, D. Wang, F. Li, B. Liu and H. Cheng, *ACS Nano*, 2010, **4**, 5835.
28 K Zhang, L. Zhang, X. S. Zhao and J. Wu, *Chem. Mater.*, 2010, **22**, 1392.
29 S. Goswami, U. N. Maiti , S. Maiti , S. Nandy , M. K. Mitra , K. K. Chattopadhyay, *Carbon*, 2011, **49**, 2245.
30 S. Stankovich, D. A. Dikin, G. H. B. Dommett, K. M. Kohlhaas, E. J. Zimney, E. A. Stach, R. D. Piner, S. T. Nguyen and R. S. Ruoff, *Nature*, 2006, **442**, 282.
31 G. Yu, L. Hu, N. Liu, H. Wang, M. Vosgueritchian, Y. Yang, Y. Cui and Z. Bao, *Nano Lett.*, 2011, **11**, 4438.
32 H. Wang, L. Bian, P. Zhou, J. Tang and W. Tang, *J. Mater. Chem. A*, 2013, **1**, 578.
33 H. Wang, E. Zhu, J. Yang, P. Zhou, D. Sun and W. Tang, *J. Phys. Chem. C*, 2012, **116**, 13013.
34 Y. Liu, E. Zhu, L. Bian, J. Hai, J. Tang and W. Tang, *Mater. Lett.*, 2014, **118**, 188.
35 S. Li, L. Qi, L. Lu and H. Wang, *RSC Advances*, 2012, **2**, 6741.
36 Y. Xu, H. Bai, G. Lu, C. Li and G. Shi, *J. Am. Chem. Soc.*, 2008, **130**,5856.
37 Y. C. Liu and B. Hwang, *Synth. Met.*, 2000, **113**, 203.
38 C.-Y. Su, Y. Xu, W. Zhang, J. Zhao, X. Tang, C.-H. Tsai, L.-J. Li. *Chem. Mater.*, 2009, **21**, 5674.
39 J. Liu, J. An, Y. Ma, M. Li and R. Ma, *J. Electrochem. Soc.*, 2012, **159**, A828.
40 H. Chen, J. He, C. Zhang, H. He, *J. Phys. Chem. C*, 2007, **111**, 18033.
41 C. Zhu, S. Guo, Y. Fang, L. Han, E. Wang and S. Dong, *Nano Res.*, 2011, **4**, 648.
42 S. W. Lee, J. Kim, S. Chen, P. T. Hammond and S. H. Yang, *ACS Nano*, 2010, **4**, 3889.
43 J. Wang, Y. Xu, J. Zhu and P. Ren, *J. Power Sources*, 2012, **208**, 138.
44 S. Stankovich, D. A. Dikin, R. D. Piner, K. A. Kohlhaas, A. Kleinhammes, Y. Jia, Y. Wu, S. T. Nguyen and R. S. Ruoff, *Carbon*, 2007, **45**, 1558.
45 Y.-T. Wang, A.-H. Lu, H.-L. Zhang and W.-C. Li, *J. Phys. Chem. C*, 2011, **115**, 5413.
46 L. Zhang, R. Zhou and X. S. Zhao, *J. Mater. Chem.*, 2010, **20**, 5983.

Table of content

Cite this: DOI: 10.1039/c0xx00000x

www.rsc.org/xxxxxx

ARTICLE TYPE

Sandwich-structured MnO_2/polypyrrole/reduced graphene oxide hybrid nanocomposites for high-performance supercapacitors

Guangqiang Han,[a] Yun Liu,[a] Erjun Kan,[b] Jian Tang,[a] Lingling Zhang,[a] Huanhuan Wang,[a] Weihua Tang*[a]

Sandwich-structured hierarchical (MnO_2, PPy)/rGO nanosheets composites exhibited a maximum specific capacitance of 404 F g^{-1} and ~ 91% of capacitance retention over 5000 cycling.